

Event Detection in Wireless Body Area Networks Using Kalman Filter and Power Divergence

Osman Salem¹, Ahmed Serhrouchni, Ahmed Mehaoua, and Raouf Boutaba², *Fellow, IEEE*

Abstract—The collected data by biomedical sensors must be analyzed for automatic detection of physiological changes. The early identification of an event in collected data is required to trigger an alarm upon detection of patient health degradation. Such alarms inform healthcare professionals and allow them to quickly react by taking appropriate actions. However, events result from physiological change or faulty measurements, and lead to false alarms and unnecessary medical intervention. In this paper, we propose a framework for automatic detection of events from collected data by biomedical sensors. The proposed approach is based on the Kalman filter to forecast the current measurement and to derive the baseline of the time series. The power divergence is used to measure the distance between the forecasted and measured values. When a change occurs, this metric significantly deviates from past values. To distinguish emergency events from faulty measurements, we exploit the spatial correlation between the monitored attributes. We conduct experiments on real physiological data set and our results show that our proposed framework achieves a good detection accuracy with a low false alarm rate. Its simplicity and processing speed make our proposed framework efficient and effective for real-world deployment.

Index Terms—Wireless body area networks, anomaly detection, reliability, fault detection, Kalman filter, power divergence.

I. INTRODUCTION

WITH the rise of elderly populations and the continual increase in average lifetime, the shortage of places in hospital and healthcare professionals lead to long waiting lines clogging emergency rooms and the demand for doctors and staff seems to never be satisfied.

The excessive congestion is caused by many patients kept under monitoring and requiring minimal attention in these facilities. Healthcare professionals are interested in remote monitoring of patients' vital signs, as well as their surrounding environment. These interests are driving the development and

Manuscript received November 5, 2017; revised March 22, 2018 and May 25, 2018; accepted May 27, 2018. Date of publication May 31, 2018; date of current version September 7, 2018. The associate editor coordinating the review of this paper and approving it for publication was I.-R. Chen. (Corresponding author: Osman Salem.)

O. Salem and A. Mehaoua are with the LIPADE Laboratory, University of Paris Descartes, 75270 Paris, France (e-mail: osman.salem@parisdescartes.fr; ahmed.mehaoua@parisdescartes.fr).

A. Serhrouchni is with the Computer Science and Network Department, Institut Mines-Télécom, 75634 Paris, France (e-mail: ahmed.serhrouchni@telecom-paristech.fr).

R. Boutaba is with the David R. Cheriton School of Computer Science, University of Waterloo, Waterloo, ON N2L 3G1, Canada (e-mail: rboutaba@cs.uwaterloo.ca).

Digital Object Identifier 10.1109/TNSM.2018.2842195

deployment of biomedical sensing for remote collection and transmission of physiological data from monitored patients.

In medical monitoring, patients are equipped with small biomedical sensors on different places of their bodies to monitor one or several physiological attributes. This set of sensors on human body is referred to as Wireless Body Area Network (WBAN). The sensors are tiny and use one of existing wireless technologies (ZigBee, Bluetooth, etc.) to transmit the measurements to a portable Local Processing Unit (LPU). The latter is usually less constrained in terms of processing power, energy and transmission range.

WBANs are great assets for both patients and professionals because they reduce healthcare costs by solving many known problems (e.g., overcapacity, excessive waiting time, sojourn time, number of nurses, etc.) mainly by reducing the number of occupied hospital beds by patients under monitoring. Various clinical conditions can be prevented or better monitored using WBANs, where the collected data in real-time can be used to follow the evolving state of the remotely monitored patient, for early detection of clinical emergency and fast reaction for eventually saving the life of the monitored patient [1].

In addition to cost reduction, the pervasive monitoring using WBANs enables patients mobility and freedom of movement, by allowing them to perform their daily life activities while being monitored. The in-network processing of collected data from different sensors allows to raise an alarm upon detection of unusual change associated with potential diseases, and quickly warn healthcare professionals to prescribe the appropriate medical care. For example, high blood pressure is an important indicator of cardiovascular diseases (heart attack), an oxygenation ratio (SpO₂) lower than 95% is an indication of asphyxia, insufficient oxygen (hypoxia) or pneumonia.

Several medical sensors with limited wireless transmission range are available today in the market at affordable price (Shimmer [2], etc.). Available sensors are able to monitor different physiological attributes [3], such as Heart Rate (HR), PULSE, SpO₂, Respiration Rate (RR), Body Temperature (T°), Blood Pressure (BP), Galvanic Skin Rate (GSR), Blood Glucose Level (BGL), ElectroCardioGram (ECG), ElectroMyoGram (EMG), ElectroEncephaloGram (EEG), etc. Most of existing sensors gather and transmit sensed data without processing to remote devices for the purpose of detecting events associated with emergency condition.

Pervasive healthcare services require the development of real-time applications for the detection of emergency situations, such as the detection of the myocardial ischemia which precedes heart attacks (or infarctions). The early detection

prevents serious complications and damage of the heart by therapies using anticoagulants or Percutaneous Coronary Intervention (PCI) that reestablishes the normal blood flow in the obstructed coronary artery.

However, the small size and weight of the used sensors, their limited resources [4] make them susceptible to various sources of environmental noise [5], [6] and malfunctions, including hardware faults, corrupted sensors, energy depletion, errors in the measurements, mis-calibration, electromagnetic interference, signal fading, disrupted connectivity, patient's sweating, dislocation, compromised sensors [7], etc. These issues may lead to unreliable measurements [8], and consequently wrong diagnoses and inappropriate treatments.

The above issues make the monitoring system unreliable [9]–[12] which may threaten the life of monitored patients. They may result in a high rate of false alarms affecting the trust level in such monitoring system, where reliability is extremely important to ensure accuracy in the medical domain [13]. Chipara *et al.* [5] show that sensing components are the first source of unreliability in WBANs, and such monitoring system will be rejected by healthcare professionals and patients if not reliable. Consequently, faulty measurements must be detected and isolated to ensure the accuracy of medical diagnosis system.

A mechanism that allows to detect and filter out inaccuracies in the collected data is of paramount importance. However, the accurate analysis of different biomedical signals is computationally complex and requires significant processing power unavailable in existing tiny WBAN devices. Real time processing using lightweight algorithms is required to detect abrupt deviations in data and to distinguish between a clinical emergency and faulty measurements. Both cases (faulty and emergency) induce measurements that deviate from normal behavior, and should be accurately detected and classified. Accordingly, an online anomaly detection mechanism is required to identify abnormal patterns as a first step, and to distinguish clinical emergency from faulty measurements as a second step. Such detection mechanism is crucial for reliable operation of medical WBANs in the detection of emergency situations.

The main contribution of this paper is a novel framework for anomaly detection in collected data by biomedical sensors to distinguish faulty measurements from clinical emergency. The proposed framework is lightweight and intended to achieve detection in WBAN after the analysis of collected data by sensors on the LPU. Our framework uses Power Divergence (PD) to measure the distance between current and predicted reference records using Kalman Filter (KF). The value of PD increases when the measured record deviates from the reference record. As the residual time series of PD can be approximated by normal distribution with zero mean $N(0, \sigma^2)$ [14], we use a robust version of z-score to detect deviations. The distinction between deviations generated by health degradation and faulty measurement is achieved through correlation analysis of monitored physiological attributes.

The paper is structured as follows. Section II discusses related work. Section III describes our proposed framework. Section IV presents our experimental evaluation results.

Finally, Section V concludes the paper and outlines future research directions.

II. BACKGROUND AND RELATED WORK

A number of systems for remote monitoring of patients have been designed, developed and deployed for gathering vital signs at home and outdoor, such as: MEDiSN [1], CodeBlue [15], Medical MoteCare [16], Vital Jacket [17]. Some comprehensive survey studies of medical applications using Wireless Sensor Networks (WSNs) are provided in [18] and [19].

However, the collected data by WBANs usually have low quality and poor reliability, due to interference, errors, incorrect readings, environmental noise, missing values, inconsistent readings, damaged sensors, malicious injected data, etc. Different approaches for anomaly detection have been proposed and applied in WSNs to detect abnormal deviations. Existing solutions in the literature stem from different disciplines such as statistical methods, information theory and Machine Learning (ML).

Statistical methods can be classified into 2 categories: parametric and non-parametric methods. Parametric methods assume a known distribution of collected measurements, having the parameter θ_1 before the change and another parameter θ_2 after the change point. Non-parametric methods do not assume a specific distribution for values, and use distance between data points to measure the deviation between them.

Information theory focuses on determining the relevance of a certain data set using measurements such as the entropy [20], e.g., if all observations belong to the same class, the entropy is equal to zero, but once the observations are scattered in different classes, the entropy approaches one.

ML algorithms build a classification model to distinguish normal data from anomalous data by separating them into 2 classes. Various algorithms have been applied, such as Bayesian Network (BN [21]), Decision Tree (DT [22]), K-Nearest Neighbor (KNN [23]), Support Vector Machine (SVM [24]), etc. Such algorithms generate a classification model based on correlational and statistical analysis of training data set, and the derived model is applied to classify test instances as either normal or abnormal.

ML algorithms require labeled data with balanced classes to build the classification model. However, training data are often skewed (unbalanced classes) or even unavailable in practice. Furthermore, the computational complexity of deriving such models adds significant load and consumes the scarce resources, e.g., quickly depleting the limited LPU energy. These problems (training data and complexity) make the derivation (and the update) of classification model a challenging task, and are avoided in our proposed approach.

A comprehensive analysis of modern fault and outlier detection techniques for WSNs is presented in [25]. Several types of irregular readings have been captured and extracted from WSN data including single spikes, long duration spikes resulting from noisy environments, and continuously anomalous line fluctuations. To simplify the classification of WSN sensor fault types, Sharma *et al.* [26] categorize faulty measurements into

short faults, sporadic faults and constant faults. They found that most existing fault detection methods fail to detect long, short or constant faults with low intensity. Our proposed approach is able to detect all types of anomalies and to discern faulty measurements from health degradation.

Jurdak *et al.* [27] define the common types of anomalies in WSNs as: network anomalies, sensor anomalies and data anomalies. Their detection is achieved by building a model to represent normal data, and any heavy deviation from the established normal profile will be considered as anomaly. Usually, the normal measurements follow the same distribution, and the abnormal values (outliers) are generated by another distribution or require changes in statistical parameters in the distribution function. Our approach is similar to that in [27], in that we derive a reference record (or normal profile) and we measure the distance between measured and reference records to detect anomalies.

Chen and Juang [28] propose a score based approach for anomaly detection in WSNs, which is based on Hampel filter and Kernel Density Estimator (KDE) to identify outliers. However, their approach does not take into account the correlation between monitored attributes. The physiological attributes are heavily correlated in time and space. Ignoring the correlation through univariate analysis for anomaly detection may lead to false negatives, because each individual attribute may not exhibit an anomalous value [29]. Miao *et al.* [30] propose a failure detection approach for WSNs, which exploits correlations to detect abnormal sensors and to uncover failed nodes.

A common problem with the majority of existing anomaly detection approaches is the lack of consideration of both spatial and temporal correlations between monitored physiological attributes. Previous work focuses on temporal correlations without considering spatial relationships among attributes. To increase the detection accuracy, the spatio-temporal dependencies must be exploited to distinguish between errors and medical emergencies, where measurements tend to be correlated in time and space, and errors are usually uncorrelated with other attributes.

Zhang *et al.* [31] note that only limited research makes explicit use of spatial and temporal correlations for outlier detection. Subramaniam *et al.* [32] proposed an anomaly detection system in the sensor, system in the sensor, which maintains a random samples of its measurements to estimate the probability distribution of normal measurements. A measurement that does not follow the same distribution is considered abnormal. Our approach differs from theirs in three ways. First, we do not assume that measurements follow a known distribution. Second, we identify anomalies with respect to sequential data smoothing (not only random samples) and adaptive processing of the normal model. Third, we take into account spatial correlations between the data from different sensors (not only temporal correlations).

Wu *et al.* [33] proposed a localized technique to distinguish between events and outliers data by exploiting the spatial correlations among measured values by neighboring sensors. Each sensor fills a vector of measured data by its neighbors (overhearing), and applies z-score on a transform of the values in

the vector to identify faulty measurements. Their approach differs in two ways. First, they assume redundant sensors measuring the same parameter, which is difficult in medical deployment of sensors. Second, they exploit only the spatial correlations and do not consider the temporal correlations between measurements to identify outliers.

Ni and Pottie [34] proposed a data fault detection approach in sensor networks using a hierarchical Bayesian spatiotemporal (HSBT) technique, which assumes the existence of such correlations without explicitly calculating or analyzing its variation. They use Bayesian model to detect specific phenomena and use Maximum A Posteriori (MAP) to detect faults. Their approach differs from ours in three ways. First, they assume prior knowledge of an existing phenomenon to distinguish with faulty measurements. However, in medical monitoring, these phenomena are not strictly defined since they depend on several parameters which are specific to the monitored patient (age, length, weight, health condition, etc.). Second, they require known data distribution for a specific phenomenon to build the model, however physiological parameters do not follow a specific distribution. Third, they assume linear deployment of sensors, which is hard in WBANs, especially with movements of the monitored patient.

Yu *et al.* [35] used an improved autoregressive moving average model for intrusion detection in WSNs without considering spatial correlations. Mojarad *et al.* [36] proposed an anomaly detection method that ignores temporal correlations by constructing clusters regrouping sensors within predefined similarity threshold. Measurements that do not belong to any cluster are considered anomalies. In our work, we exploit the spatio-temporal correlations analysis to reduce the computational complexity and to discern faulty from health emergencies.

O'Reilly *et al.* [37] survey the few existing correlated methods (centralized and distributed) for anomaly detection. Bettencourt *et al.* [38] propose a distributed anomaly detection scheme for WSNs, where each sensor learns the distribution of its measurements and the distribution of the difference between its measurements and the measurements of its neighbors. In the detection phase, the sensor compares the current measurement with the previously derived distributions to identify deviations using a significance test.

Bao *et al.* [39] exploit only the spatial correlations to propose a trust-based management scheme for intrusion detection in WSNs. They focus on the discrimination between two classes (malicious and event) without considering permanent faults. Illiano and Lupu [7] also exploit only the spatial correlations to detect malicious data injections in WSNs. The similarity check in their estimation based framework allows them to identify compromised sensors. They use linear regression to derive their estimation models and to reduce spatial and temporal complexity. However, they also note that events cause unpredictable changes in spatial patterns and more sophisticated regressions need to be investigated.

Liu *et al.* [40] propose a distance based method to identify insider malicious sensors, while assuming that neighbor nodes monitor the same attributes. Each sensor receives packets sent by neighbor sensors due to the broadcast nature

of the network. Therefore, each sensor is able to monitor its one hop neighbors and uses Mahalanobis Distance (MD) between measured and received multivariate instances from neighboring sensors to detect anomalies in a distributed manner. Chen *et al.* [41] use graph theory to propose a fully distributed anomaly detection system. However, it is not practical in medical WBAN applications to use several sensors that are monitoring the same parameter for anomaly detection.

Another attempt to capture spatio-temporal correlations was reported in [42]. It uses regression to build two models using previous observations. However, as the model keeps a sliding window of past collected instances, it is subject to false alarms if outliers are not discarded from the training data that are used to build the model. In [43], the MD has been used to classify electronic products as healthy or unhealthy.

In our paper, we build on previous work to devise more lightweight and more robust techniques specifically for WBANs. We start by deriving a normal profile (denoted by reference record) through the use of KF model, which forecasts the baseline using past records. The reference record is not static and will be updated after each measurement. To measure the dissimilarity between multivariate vectors (reference and measured), we used the Power Divergence (PD) to detect deviations from the established baseline model by KF for the current instant. When a deviation is detected, we conduct spatio-temporal correlations analysis between physiological attributes to distinguish faulty measurements from medical emergency situations. Faulty measurements do not trigger false alarms and only correlated changes raise a medical alarm. Compared to previous work, the originality of our approach lies in the derivation (and update) of a reference model, computing the distance between measured and reference records, detecting deviations in the derived distance using robust techniques, and exploiting the spatio-temporal correlations to reduce false alarms.

III. PROPOSED APPROACH

We consider a general deployment scenario, where m wireless nodes with restricted resources are placed on multiple different positions of the body of monitored patient. These small sensors are used to collect and transmit data to the LPU (as shown in Figure 1), which is a central processing device with more resources and higher transmission capabilities than nodes. The collected data are processed in the LPU to detect abnormal patterns, isolate faulty measurements and to raise alarms for healthcare professionals upon the detection of a physiological change. We seek to detect abnormal values associated with clinical emergency (events) and to reduce false alarms triggered by faulty measurements.

Let $A = (A_1, A_2, \dots, A_m)$ be a multivariate time-series associated with multiple physiological attributes, where $A_m = (x_{1,m}, x_{2,m}, \dots, x_{n,m})^T$ is a set of n observations of the m^{th} attribute. A_m is the column m in the matrix A given in equation (1). L_n represents an instance vector at time instant n , where $L_n = (x_{n,1}, x_{n,2}, \dots, x_{n,m})$ is the

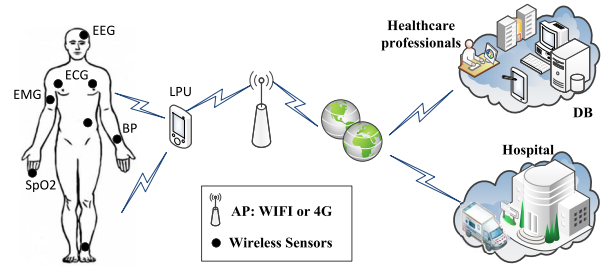


Fig. 1. WBAN in medical deployment scenario.

n^{th} line in the data matrix A .

$$A = \begin{matrix} & A_1 & A_2 & A_3 & \dots & A_m \\ L_1 & x_{1,1} & x_{1,2} & x_{1,3} & \dots & x_{1,m} \\ L_2 & x_{2,1} & x_{2,2} & x_{2,3} & \dots & x_{2,m} \\ \vdots & \vdots & \vdots & \vdots & \ddots & \vdots \\ L_n & x_{n,1} & x_{n,2} & x_{n,3} & \dots & x_{n,m} \end{matrix} \quad (1)$$

To detect deviations in received records, we use the distance based method to compare the current distribution of measured record L_t with a reference distribution of record L_t^{ref} . With one or many abnormal values in measured records, the distance between two sets of probability values will increase significantly. For two discrete probability distributions $P = (p_1, p_2, \dots, p_m)$ and $Q = (q_1, q_2, \dots, q_m)$, with $p_i \geq 0$, $q_i \geq 0$, the sum of all elements in each vector is equal to one:

$$\sum_{i=1}^m p_i = \sum_{i=0}^m q_i = 1 \quad (2)$$

Let P denotes the reference distribution and Q represents the distribution of the current measured record. To derive the probability distribution Q from the record L_n , we first compute the sum of all elements in L_n , then the probability q_i is calculated as the ratio of each attribute to the sum of all values:

$$q_i = x_{n,i} / \sum_{j=1}^m x_{n,j} \quad (3)$$

The same goes for the derivation of the reference distribution P from the reference record $L_n^{\text{ref}} = (z_{n,1}, \dots, z_{n,m})$:

$$p_i = z_{n,i} / \sum_{j=1}^m z_{n,j} \quad (4)$$

The reference record $L_n^{\text{ref}} = (z_{n,1}, \dots, z_{n,m})$ contains the normal values for each monitored physiological attribute. The distance between a reference distribution P (derived from the baseline record L_n^{ref}) and the current distribution Q (derived from the current record L_n) is analyzed to detect deviations in measured data.

To detect anomalies in the measured record L_n , we start by deriving the baseline (or reference) record L_n^{ref} in order to calculate the distance between reference and current measurements. To derive the reference record of the monitored attributes, we use KF, which allows to estimate the current measurements based on previous measurements and the state of the model. KF is able to capture the baseline of the time

series and to derive whole fields in L_n^{ref} . To compare the two records (L_n^{ref} and L_n), the probability distributions P and Q are derived and used as input for the distance metric $PD(P||Q)$ (given in equation (13)). The PD is used to measure the deviation between current and reference (forecasted by KF) distributions.

For clarification, let us consider a system with 4 monitored attributes: HR, Pulse, RR and SpO2, where measured values at time n are stored in the vector $L_n = (x_{1,n}, x_{2,n}, x_{3,n}, x_{4,n}) = (80, 79, 15, 95)$. The baseline L_n^{ref} contains the predicted values (by KF) for each attribute at time instant n , $L_n^{ref} = (z_{1,n}, z_{2,n}, z_{3,n}, z_{4,n}) = (80, 79, 15, 95)$, where $z_{i,n}$ is the predicted value for $x_{i,n}$. The vector $Q = (0.3, 0.29, 0.06, 0.35)$ is derived from L_n , and the vector $P = (0.3, 0.3, 0.05, 0.35)$ is derived from L_n^{ref} as given in equations (3) and (5).

In fact, when a physiological change spans over multiple intervals $[t, t + w]$, the PD will deviate from zero and may generate w continuous spikes during the whole change interval. The residual of the divergence metric (PD) can be approximated by normal distribution, where a robust version of zscore is applied to detect deviations.

Our proposed approach involves 3 steps: 1) time series forecasting using KF; 2) computing the distance between reference and measured records using power divergence; 3) analysis of the residual using robust zscore to detect deviations. We detail these 3 steps in the following subsections.

A. Kalman Filter (KF)

KF is an optimal estimation algorithm used to estimate parameters of interest from indirect, inaccurate and uncertain observations. KF is well suited for online and real-time processing, where new measurements can be processed as they arrive, and without storing observations or past estimates. The KF is the best linear estimator that minimizes the mean-squared error of the estimated parameters.

KF produces accurate predictions for linear systems, and it may have problems with stability of prediction for complex nonlinear system. Many physiological parameters (ECG, EEG, etc.) have non-linear and highly dynamic measurements. The Extended Kalman Filter (EKF) can be applied to a linearized version of these signals with loss of optimality, where the prediction is inaccurate in practice and it is not very stable with slow convergence to a good solution. The Unscented Kalman Filter (UKF) with the Unscented transformation describes the nonlinear system better than the linearization, and rapidly converges to a good solution. However, the EKF and UKF may become unstable and results may be biased.

Zjajo [44] compares the estimation accuracy of readings from temperature sensors using KF, EKF and UKF. He found that UKF achieves the best precision and slightly outperforms KF and EKF, at the cost of computational complexity. In our approach, we used KF because of its computational efficiency, and its small memory requirements. It requires less processing power than EKF and UKF, and therefore it is more convenient for online processing than UKF in a constrained resource environment such as ours. Furthermore, the proposed system is

intended to analyze the vital signs (RR, SpO2, Pulse, HR, etc.), which exhibit slow changes in a small time interval.

KF is a simple predictive model used to derive the baseline of measurements through the estimation of the current measurements based on previous measurements. The estimated values are very effective for anomaly detection, especially when looking at the difference between forecasted baseline and measured values.

KF has been used in a variety of applications, such as noise filtering, sub-space signal analysis, feature extraction, indoor localization, etc. We use KF here for its baseline approximation with a lightweight computation complexity. KF assumes the following linear models with additive Gaussian white noise:

$$\begin{cases} S_t = FS_{t-1} + BU_{t-1} + W_{t-1} & W_t \sim N(0, Q) \\ Z_t = HS_t + V_t & V_t \sim N(0, R) \end{cases} \quad (5)$$

S_t are the hidden states, Z_t are the predicted measurements, F is the state transition matrix, B is the control input matrix, U_k is the control vector, H is the observation matrix used to map state space into the observed space, W_t and V_t are white Gaussian noise with zero mean and covariance matrix Q and R :

$$E[W_i W_j^T] = Q\delta(i - j) \text{ and } E[V_i V_j^T] = R\delta(i - j) \quad (6)$$

$$E[W_i V_j^T] = 0 \quad \forall i, j \quad (7)$$

$\delta(i - j)$ is the dirac delta function which has zero value everywhere except when $i = j$, as given in equation (8):

$$\delta(i - j) = \begin{cases} 1 & \text{if } i = j \\ 0 & \text{Otherwise} \end{cases} \quad (8)$$

The prediction Z_t of X_t at time instant t given the past measurements X_1, X_2, \dots, X_{t-1} is performed in two phases: prediction and correction. In fact, we use the notation X_t for simplification, where X_t represents the measured value of a given attribute at time instant t , which has been previously denoted by $x_{t,i}$ for the i^{th} attribute and where the past measurements are $x_{1,i}, x_{2,i}, \dots, x_{t-1,i}$. In the prediction phase, KF estimates the next state and the predicted covariance matrix of the state:

$$\begin{aligned} S_t &= FS_{t-1} + BU_{t-1} \\ P_t &= FP_{t-1}F^T + Q \\ Z_t &= HS_t \\ e_t &= X_t - Z_t \end{aligned} \quad (9)$$

where S_t and P_t are the estimate of the system state and state transition covariance matrix before the measurement update and correction. In the estimation phase, KF updates its forecasting parameters and predicts the value of the next measurement:

$$\begin{aligned} K_{t+1} &= \frac{P_t H^T}{H P_t H^T + R} \\ S_{t+1} &= S_t + K_{t+1}(X_{t+1} - H S_t) \\ P_{t+1} &= (I - K_{t+1}H)P_t \end{aligned} \quad (10)$$

where K_t is the KF gain. We can notice the impact of noise in the update of state covariance P_{t+1} in equation (10).

The values of F , B and H distinguish different KF models, such as systems that take velocity and acceleration into account to derive distance for indoor localization. In the simplest prediction model of KF, we set A and H to identity and B to zero, because we know that the measurement is composed of the state value and some noise. The system state becomes a vector storing the average of the measurements. We also set the Q , R and P_0 to 0.1 and S_0 to 0 in similar manner as in [45]. The used model to predict the state of the model in equation (10) becomes:

$$S_t = S_{t-1} + K_t \times (X_t - Z_{t-1}) \quad (11)$$

Therefore, the predicted $Z_t = I \times S_t$ value of X_t is:

$$Z_t = Z_{t-1} + K_t \times (X_t - Z_{t-1}) \quad (12)$$

After the derivation of reference time series using KF, we analyze the distance between measured and forecasted records using PD.

B. Power Divergence (PD)

PD [46] measures the distance between two probability distributions P and Q as given in equation (13). Its value is near zero for similar distributions, and increases significantly when the distributions diverge. PD is a general form of divergence measures, where Kullback Leibler (KL [47]), Hellinger Distance (HD [48]), chi-square (χ^2 [49]) and other distances, can be derived from PD by changing its parameter (β). PD is given by:

$$\begin{aligned} PD(P||Q) &= \frac{E_P \left[(P/Q)^{\beta-1} \right] - 1}{\beta(\beta-1)} \\ &= \frac{\sum_{i=1}^m p_i (p_i/q_i)^{\beta-1} - 1}{\beta(\beta-1)} \end{aligned} \quad (13)$$

where $E_P[\cdot]$ is the expectation with respect to the posterior probability distribution P . PD presents some interesting special cases when changing its parameter β . For $\beta = 0.5$, PD is proportional to HD [46] ($PD = 4 \times HD$):

$$HD(P, Q) = \frac{1}{2} \sum_{i=1}^m (\sqrt{p_i} - \sqrt{q_i})^2 \quad (14)$$

While for $\beta = 2$, PD is proportional to χ^2 ($PD = \frac{1}{2} \times \chi^2$), where:

$$\chi^2(P||Q) = \sum_{i=1}^m \frac{p_i^2}{q_i} - 1 \quad (15)$$

The power divergence family in equation (13) is undefined for $\beta = 0$ or $\beta = 1$. However these cases are defined as follows:

$$\begin{aligned} \lim_{\beta \rightarrow 0} PD(P||Q) &= KL(Q||P) \\ \lim_{\beta \rightarrow 1} PD(P||Q) &= KL(P||Q) \end{aligned} \quad (16)$$

The reference distribution P is derived from the forecasted record using KF and the distribution Q from the measured record as given in equation (2). However, as the PD is

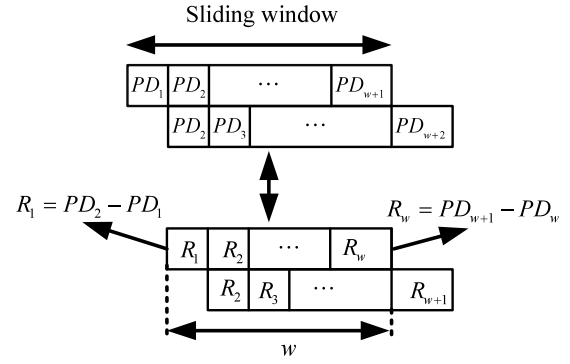


Fig. 2. Sliding window and residual.

asymmetric ($PD(P||Q) \neq PD(Q||P)$), we have observed that using the reverse distance metric, in which P is the distribution of the current record and Q is of the reference record, the distance reacts stronger to change than the forward distance (P as reference and Q as the current distribution). Therefore, we conduct our experiments using the backward distance.

To detect deviations in PD, a threshold is required to separate normal from abnormal distance values. When the distance is larger than the threshold, a hypothesis change is assumed and an alarm is triggered. However, with the real time variation of physiological attributes due to physical activities, the distance values will fluctuate over time and a static threshold is neither practical nor efficient.

To properly define a dynamic threshold, the residual time series R_i associated with the difference between the current and the previous value of PD ($R_i = PD_i - PD_{i-1}$) is derived, and follows an approximately normal distribution with mean μ and variance σ^2 . We use a robust version of zscore to detect deviations.

C. Robust Zscore

The zscore uses the mean (μ) and standard deviation (σ) of the residual time series ($R_i^w = \{R_{i-w}, \dots, R_i\}$) to measure the distance between a data point and the mean:

$$z = \frac{R_{i+1} - \mu}{\sigma} \quad (17)$$

We use a sliding window of past w values of residual time series (R_i) as shown in Figure 2, to calculate μ and σ . However, the data in the sliding window is not reliable and may contain outliers, which disrupt the estimated values for these statistical parameters.

When outliers are inside the sliding window, they dominate and pull the statistical parameters (μ and σ) toward them, and this leads to swamping and masking. Masking hides outliers and swamping declares normal values as outliers. Therefore, instead of removing the outliers from the estimation process, we use robust statistical parameters by replacing μ and σ by median (Q_2) and Median Absolute Deviation (MAD) as proposed in [50]:

$$rz = \frac{R_{i+1} - Q_2}{1.4826 \times MAD} \quad (18)$$

where Q_2 (the middle of sorted vector) and MAD are calculated as follows:

$$Q_2 = \text{med}(R_i^w) = \begin{cases} R_{\frac{w+1}{2}} & \text{if } w \text{ is odd} \\ \frac{1}{2} \left(R_{\frac{w}{2}} + R_{\frac{w}{2}+1} \right) & \text{if } w \text{ is even} \end{cases} \quad (19)$$

$$MAD = \text{median}\{|R_i^w - Q_2|\} \quad (20)$$

The robust zscores are used to test if the value of R_{i+1} is normal or abnormal, where 95% of normal data lies within a score of 1.96. When $|rz|$ is greater than 1.96 ($|rz| > 1.96$), a deviation is detected. It is important to note that data in sliding window have zero or near zero MAD under normal condition, and we use $MAD = \max(MAD, c_1)$ to eliminate false alarms, where c_1 is a predefined constant greater than zero.

The robust zscore can only detect spatial deviations, without any information on the underlying attributes responsible of change. To identify the abnormal attributes, the KF forecasting procedure can be exploited to pinpoint temporal deviation in each attribute, by checking the Euclidean distance between forecasted $z_{i,j}$ and measured values $x_{i,j}$. When this difference is greater than $p\%$ of the forecasted value (equation (21)), a deviation is considered in the j^{th} attribute.

$$e_i = |x_{ij} - z_{ij}| \geq p \times z_{ij} \quad (21)$$

The value of p must be chosen as a tradeoff between false alarms and detection accuracy. A large value of p will decrease the false alarms and the detection accuracy, and a small value of p will increase the false alarms and the detection accuracy. The optimal value of p was determined empirically, where an upper limit of normal fluctuation between forecasted and measured values is set to 10% of the baseline. In fact, forecasting using KF takes into account past measurements to estimate the next one, and as the monitored vital signs do not heavily change (no more than 10%) between two consecutive measurements (1 second), the measured value should not exceed 1.1 of the forecasted baseline, as given in equation (22):

$$|x_{ij}/z_{ij}| \leq 1.1 \quad (22)$$

As physiological parameters are heavily correlated, and faulty measurements are spatially unrelated with other attributes, we use this correlation to distinguish faulty from emergency situations. If the number of deviated attributes is greater than r ($nb \geq r$), the deviation is generated by physiological change and the LPU raises an alarm for healthcare professionals to quickly react. Otherwise, the LPU considers the measurement faulty and will not raise any alarm.

On one hand, increasing the value of r will decrease the number of false alarms and true positives. On the other hand, decreasing the value of r will increase the number of false alarms and true positives. Therefore, a tradeoff between reduced false alarms and high true positives is required to set the value of r . In our experiments, we set $r = 2$ to reduce false alarms while keeping high true positives. We notice that both values of r ($r = 1$ and $r = 2$) provide the same true positives with highest false alarms when $r = 1$.

IV. EXPERIMENTAL RESULTS

In this section, we present our experimental results on real physiological data set with annotations, which are publicly available from the Physionet [51] Web site. We conduct experiments over many subjects from Multiparameter Intelligent Monitoring in Intensive Care (MIMIC [52]) to analyze the detection accuracy and the false alarm rate. The aim of MIMIC is to provide researchers with publicly annotated database of Intensive Care Unit (ICU) patients after removing protected health information. This database contains over 90 patient records, and is used in the development and evaluation of recently proposed system for patient monitoring. The average length of these records is 40 hours.

To annotate patient data set, a clinician marks critical events during the patient's sojourn. Afterward, events are confirmed by other clinicians. Annotations for alarms related to changes in the patient's status are typically available for limited number of patient's data, as this operation is time consuming. The available physiological attributes in each record depends on the clinical state of the patient, where available record may include: one or two leads of surface ECG, systolic Arterial BP (ABPsys), diastolic Arterial BP (ABPdias), mean Arterial BP (ABPmean), HR, Pulmonary Artery Pressure (PAP), PULSE, Respiration (RESP), SpO2, Body Temperature, etc.

The ECG is the electrical signal generated during heart activities (contraction/decontraction) and it is measured in mV. The BP measures the strength of blood when pushing against the blood vessels and it is measured in millimeters of mercury (mmHg) and is written as two numbers (systolic/diastolic). The HR and the PULSE measure the number of heartbeats per minute from two different places on the patient body, and they are measured in beats per minute (bpm). The PAP is the pressure the heart exerts to pump blood through arteries of the lungs. The respiration rate is the rate at which breathing occurs and it is usually measured in respirations per minute (rpm). The SpO2 measures the amount of oxygen in the blood and it is measured as a percentage (%) in non-invasive method using pulse oximetry. Due to space limitation, we present our results only on part of the data of subjects 55, 221 and 226. These records contain 7 attributes: ABPsys, ABPdias, ABPmean, HR, PULSE, RESP, SpO2. As ABPmean is derived from ABPsys and ABPdias, we focus only on five attributes: BPmean, HR, PULSE, RESP and SpO2. Annotations for those records are provided with the dataset.

Measured value of each attribute is compared with the predicted value using KF, which subsequently depends on past values and the state of the system. When the PD distance between measured and forecasted values in the record deviates from previous measurements, a temporal analysis is conducted to check the number of deviated attributes. As physiological parameters are correlated, clinical emergency induces at least r attributes, and faulty measurements are usually uncorrelated with other measurements. Afterward, we conduct performance analysis using the Receiver Operating Characteristic (ROC) and we compare the accuracy of our proposed approach with MD, SVM and decision tree (J48).

In our experiments, we set the size of the sliding window w to 10 to estimate Q_2 and MAD, with 70% of overlapping after

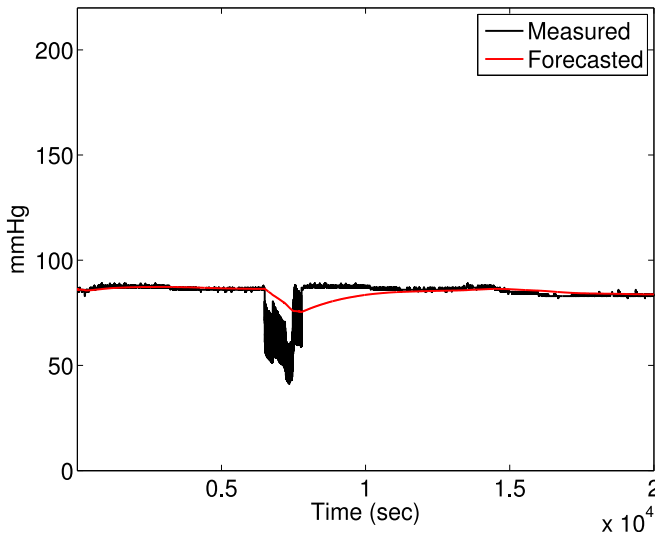


Fig. 3. Arterial Blood Pressure (ABP).

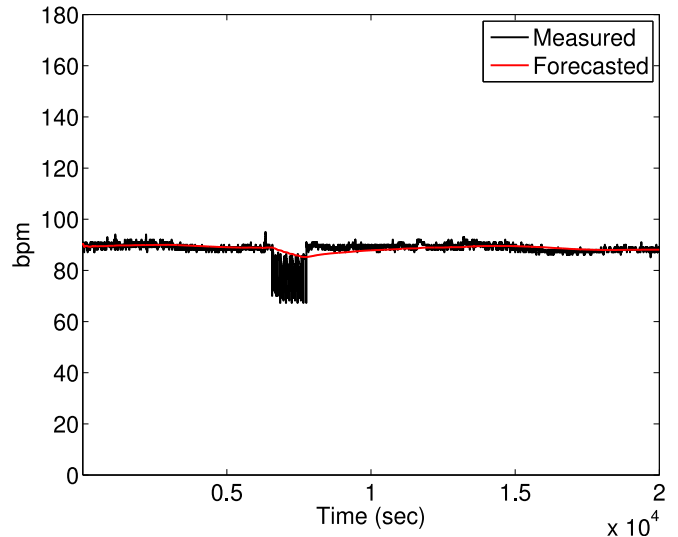


Fig. 4. Heart Rate (HR).

each step, r_z is set to 1.96 and r is set to 2. The parameters for KF are: $F = I_5$, $B = 0$, $Q = 0.001$, $H = I_5$, $R = 4$, $S_0 = 0$ and $P_0 = 1$. For the clarity of representation of the used physiological parameters in our experiments, we start by showing the variations of each attribute.

We start by focusing on part of the physiological data from subject 55, a young man of 38 years diagnosed with respiratory failure. The monitoring duration lasts for 37.5 hours. We focus only on the part of the physiological data where it cannot easily distinguish faulty measurements from clinical emergency. The variations of the ABPmean are presented in Figure 3, where ideal values for BP fall inside the interval $[80 - 120]$. By visually inspecting the variation of the BP, we can identify 1 zone of abnormal change, even outside the range of normal value. The variations of the HR are shown in Figure 4. The normal values of the HR are inside the interval $[60 - 100]$ for a healthy adult at rest. We can visually identify 1 zone of abnormal variations between 5000 and 10^4 in Figure 4.

The variations of the PULSE are shown in Figure 5. Visually, we can identify the same zone of abnormal variation in the same range. The variations of the normal respiration rate are inside the interval $[12 - 15]$. The variations for this subject are presented in Figure 6 with abnormal variations between 5000 and 10^4 containing spikes with near zero value followed by an augmentation in respiration rate.

The SpO2 represents the percentage of oxygen in blood and varies within the range $[95\% - 100\%]$. A lower value is synonymous of asphyxia, lack of oxygen and heart disease. In Figure 7, we can notice one spike with zero value near 10^4 followed by normal values. We also plot in each of the previous figures (3), 4, 5, 6 and 7 the forecasted values using the KF.

To show the correlations between monitored attributes, we depict the variations of the 5 attributes in Figure 8, where we can notice that clinical emergency induces changes in many attributes at the same time instant. However, there is no spatial correlation among monitored attributes for faulty measurements in SpO2, where its value falls down to zero without

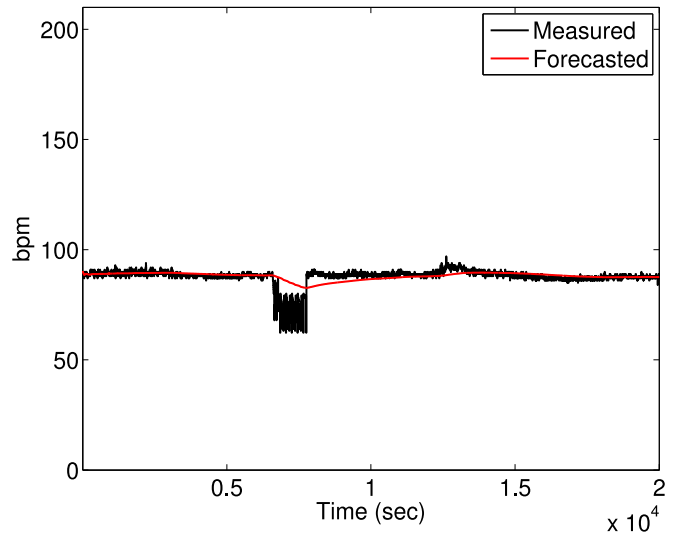


Fig. 5. Pulse.

significant changes in other attributes. It is important to note that some curves in Figure 8 are shifted to visualize the shape of their variations. We can visually distinguish 1 zone of correlated or clinical change in almost all physiological attributes of the monitored patient and 1 abnormal measurement transmitted by the SpO2 that is a spike associated with the detached sensor or the faulty measurement.

To find the optimal value for the parameter β in PD, we conduct experiments by varying the value from 0 to 100. As previously mentioned, PD is equivalent to KL for $\beta = 0$ and its variations when applied between forecasted and measured records as shown in Figure 9. The value of the KL divergence is zero for normal attributes and increases when the physiological attributes deviate. The amplitude of KL is proportional to the deviations in attributes, where a large spike associated with the abnormal value in the SpO2 can be distinguished.

Figure 10 shows the variations of HD, which is proportional to PD for $\beta = 0.5$, and is more sensitive to variations

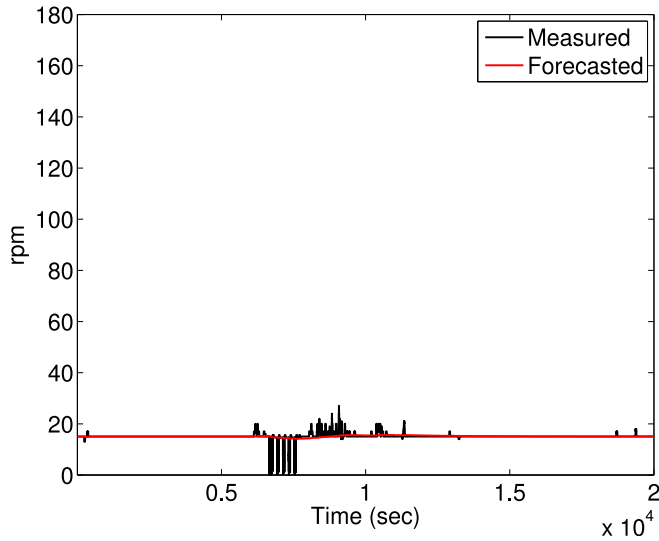


Fig. 6. Respiration Rate.

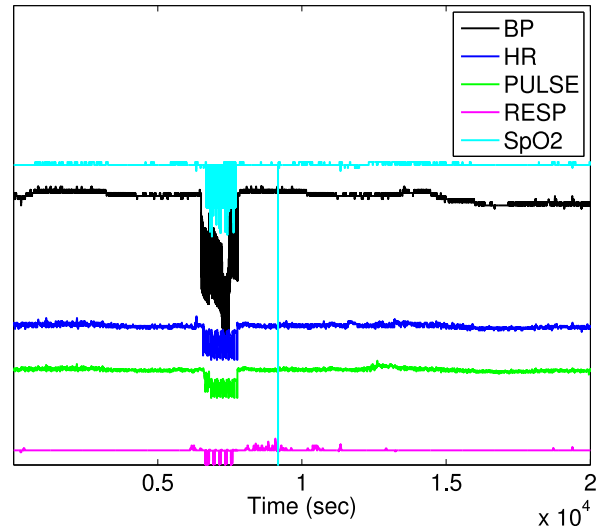


Fig. 8. Variations of 5 attributes.

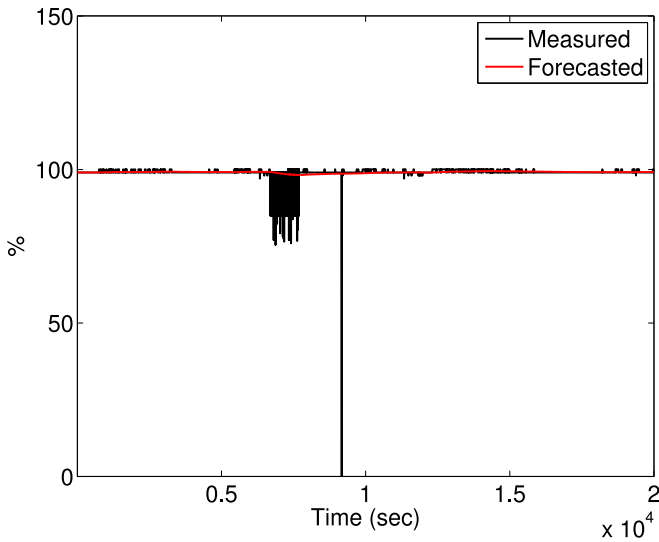


Fig. 7. Oxygenation ratio (SpO2).

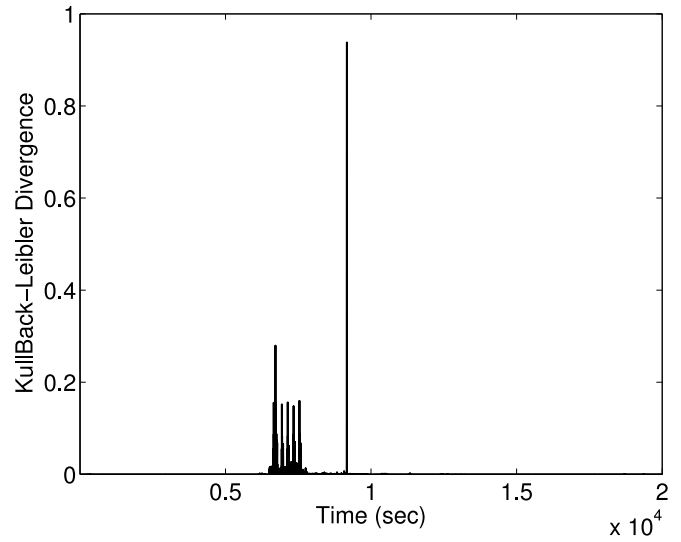


Fig. 9. KullBack-Leibler (KL).

in KL. The variations of χ^2 ($\beta = 2$) divergence are shown in Figure 11, where the amplitude of spikes associated with changes in physiological attributes is more easily distinguished from KL and HD. We notice that a large value of β makes the detection procedure more simple even with the static threshold.

We conduct a second set of experiments with different values of β to confirm the previous conclusion about the amplitude of spikes in PD and the optimal value of β . The variations of PD for β equal to 0.25, 1.5, 2.5 and 10 are shown in figures 12, 13, 14 and 15 respectively. This set of experiments confirms our previous conclusion, where the intensity of spikes associated with deviations increases with the value of β . The values of PD during physiological changes for large β become outliers and can be distinguished by outlier detection technique (z-score, p-value, boxplot, etc.) or even using a static threshold.

For $\beta \geq 2.5$, there is no significant difference in the detection system and we set *beta* to 2.5 in the rest of our

experiments. The raised alarms by power divergence for this subject are shown in Figure 16, where we can see one raised false alarm associated with the spike in SpO2. However, as this change is uncorrelated with other attributes, the associated false alarm is discarded by the correlations analysis procedure and the raised alarms with the 5 physiological attributes are shown in Figure 17.

In the second set of our experiments, we conduct the same analysis on the physiological attributes from subject 226, a man of 68 years also diagnosed with respiratory failure. The available data set containing the values of physiological attributes lasts for 31.9 hours. We start by showing the variations of each attribute with its forecasted values using the KF. The variations of the ABPmean are presented in Figure 18. In fact, we can identify 11 zones of abnormal changes by visual inspection of the variations in Figure 18. The forecasted values for the blood pressure is slightly impacted by these deviations. The variations of the HR are shown in Figure 19, where we

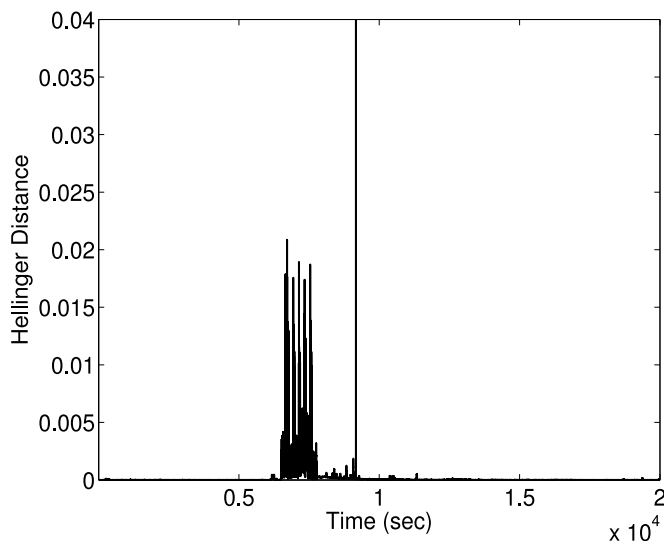


Fig. 10. Hellinger Distance (HD).

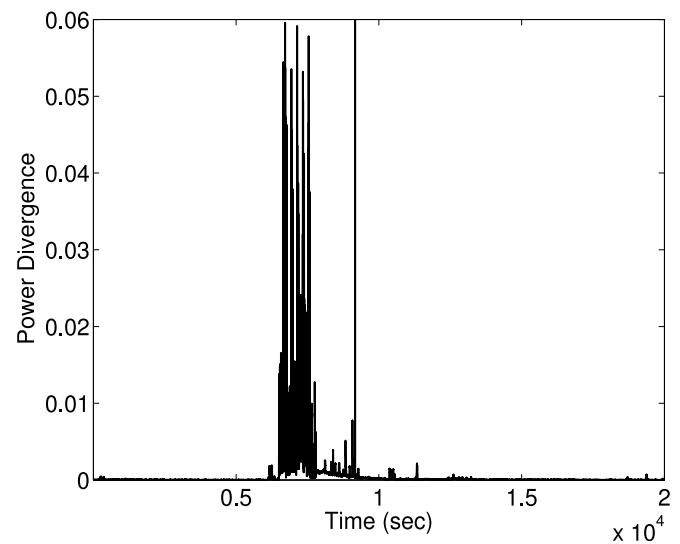
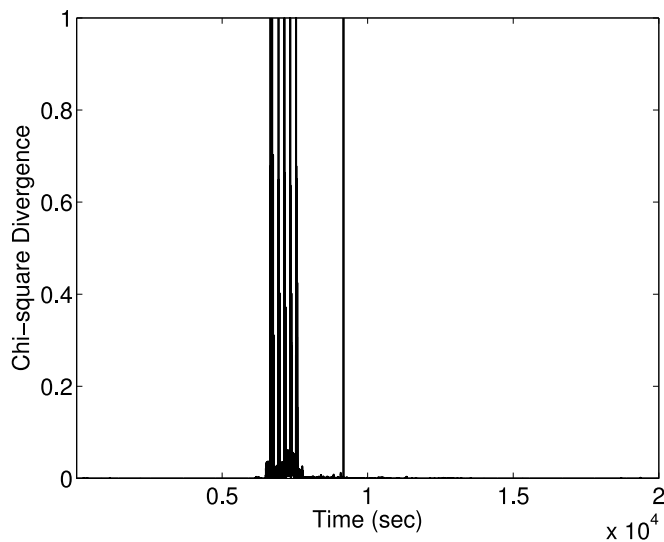
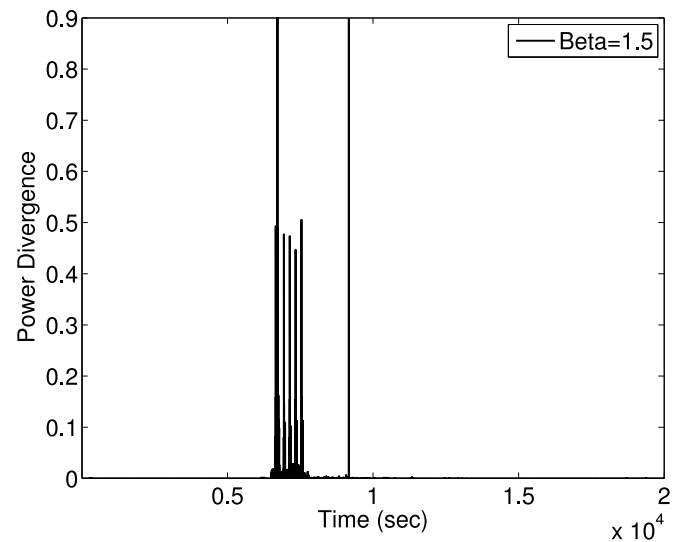
Fig. 12. PD for $\beta = 0.25$.

Fig. 11. Chi-square Divergence.

Fig. 13. PD for $\beta = 1.5$.

can identify 1 abnormal spike falling down to zero for only one sample and 11 zones of abnormal change.

Figure 20 shows the variations of measured and forecasted values of the pulse. It is measured in beats per minute (bpm) and must exhibit similar variations in the HR as they represent the same attribute monitored through two different devices. However, slight differences appear when we draw them in the same figure, and these differences are generated by faulty measurements. We can also notice one abnormal spike falling down to zero at different time instant than in Figure 19, and a difference of 4 spikes in the exiting 11 zones of changes.

Figure 21 shows the variations of the respiration rate where the mean value of respiration for the record 226 is 15 rpm with a maximum value of 55 rpm. In contrast to the previous subject, where the value of respiration rate decreases, the respiration increases for the subject 226. Figure 22 shows the variations of SpO₂, which is measured in percentage, and contains one spike with zero value for SpO₂ followed by normal

values. It is obvious that this spike is faulty due to its short duration (one value) and the fast return of the attribute SpO₂ to its normal value. It superposes with the spike with value zero in pulse, but as both attributes are measured using the same device (clips), which can be affected by the movements of the monitored patient, and when the clips is open or is not well positioned, readings are zero value or very large values (faulty).

The variations of the 5 attributes are presented in Figure 23 to highlight the correlated changes and pinpoint those associated with clinical emergency. The lack of spatial and temporal correlations can be used to detect and reject faulty measurements in monitored attributes. It is important to note, that we shift the attributes in Figure 23 for more clarity, where we multiply each attribute by a constant. The objective is to focus on the shape of variations and the presence of correlations between attributes during clinical changes. We can visually distinguish 11 zones of correlated or clinical change

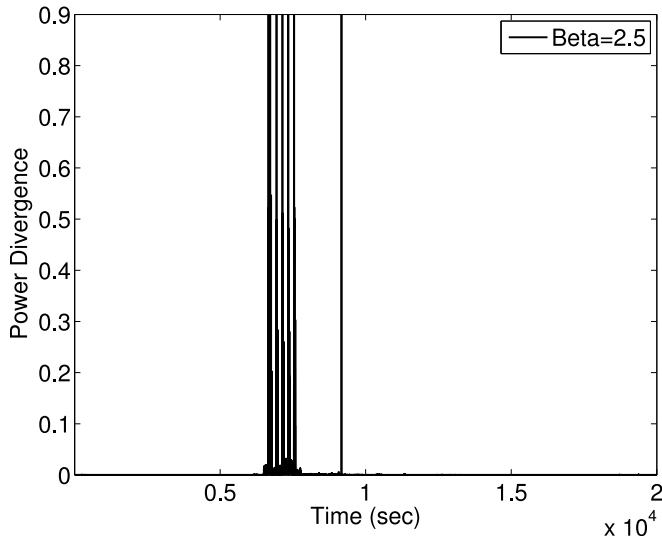
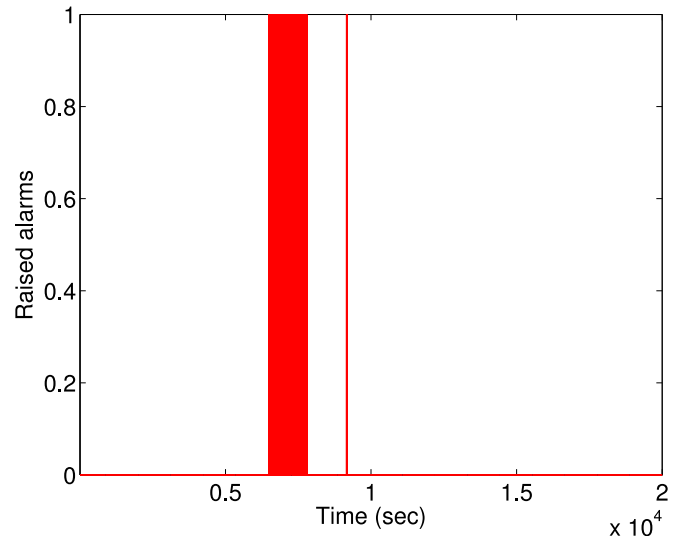
Fig. 14. PD for $\beta = 2.5$.

Fig. 16. Raised alarms by PD.

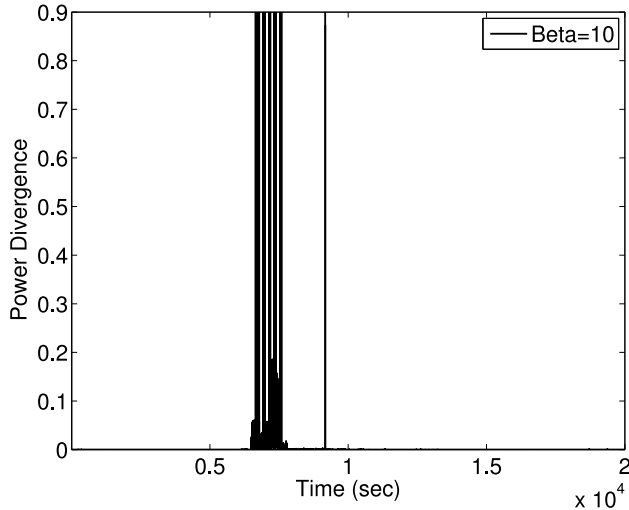
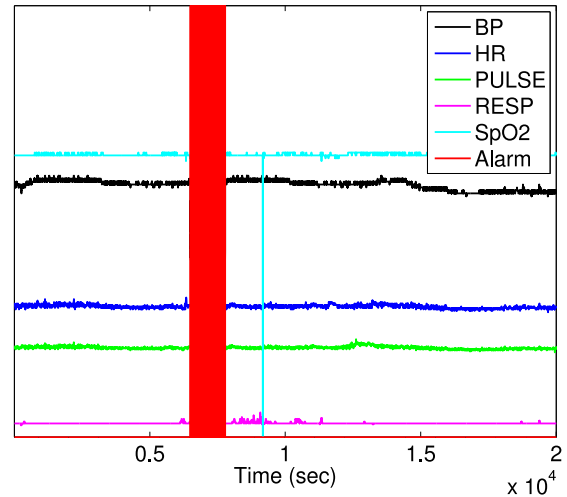
Fig. 15. PD for $\beta = 10$.

Fig. 17. Correlated change.

in almost all physiological attributes of the monitored patient. Furthermore, one abnormal measurement transmitted by HR (zero value) is uncorrelated with other attributes and is a spike associated with a detached sensor or a faulty measurement.

The PD between forecasted and measured values for physiological attributes is shown in Figure 24, where normal values are near zero values and spikes or deviations in PD are generated by changes in physiological attributes or by faulty measurements. The residual time series associated with difference between two consecutive values of PD is shown in Figure 25. The value of residual time series must be zero for normal values of PD and deviates from zero when there is a change in any measured attribute. Figure 26 shows the variations of the 5 attributes with the raised alarms after correlation analysis. As can be seen 12 alarms are generated, 11 among them are generated by clinical changes and one false alarm is generated by simultaneous changes in 2 attributes, when the values of pulse and SpO2 fall down to zero.

In the third set of experiments, we conduct an analysis on the data set from subject 221, a Female of 68 years diagnosed with Brain injury. The variations of the 5 physiological attributes are shown in Figure 27, where we can identify 4 zones of correlated changes located in the dotted boxes in Figure 28. The variations of forecasted attributes by KF are shown in Figure 29, where the 5 attributes are smoothed and abrupt deviations are discarded. The perturbations with erroneous measurements (due to patient movements causing intermittent detachment of sensors) in input data, as the 3 spikes falling to zero in SpO2 due to clips detachment (shown in Figure 26), do not disrupt the forecasting model. Furthermore, the use of robust version of zscore with robust statistical parameters (Median and MAD), prevents outliers from disrupting the decision procedure and enhances the detection accuracy by avoiding the masking and the swamping problems. Masking occurs when outliers are masked by the

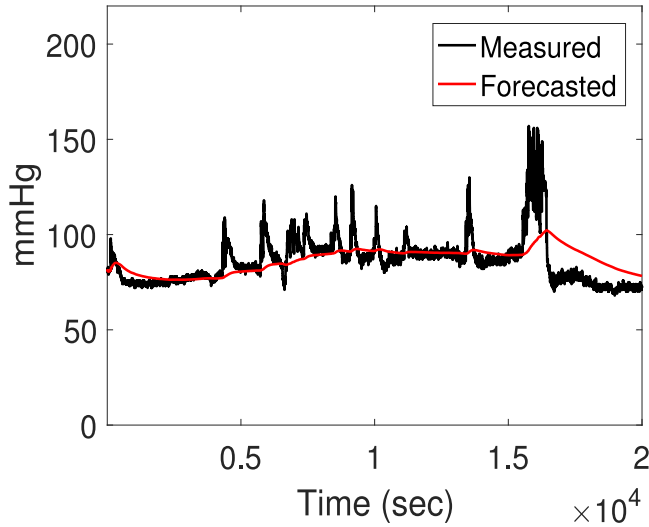


Fig. 18. Blood Pressure.

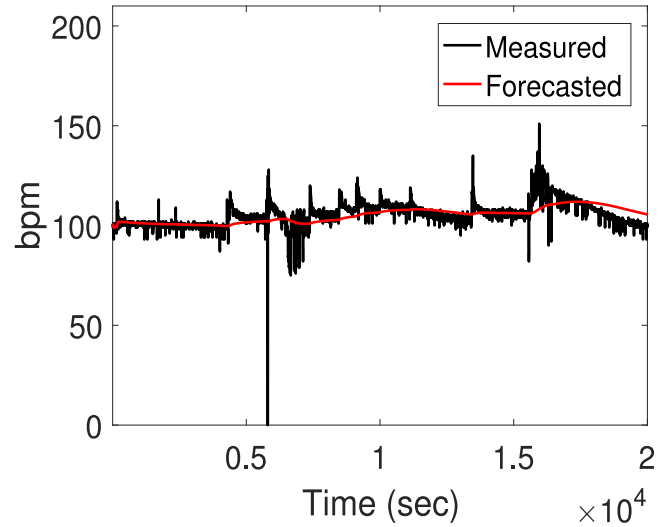


Fig. 20. Pulse.

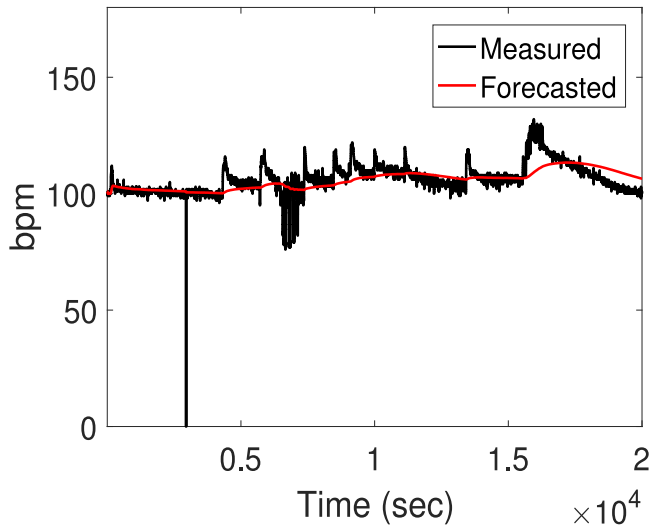


Fig. 19. HR.

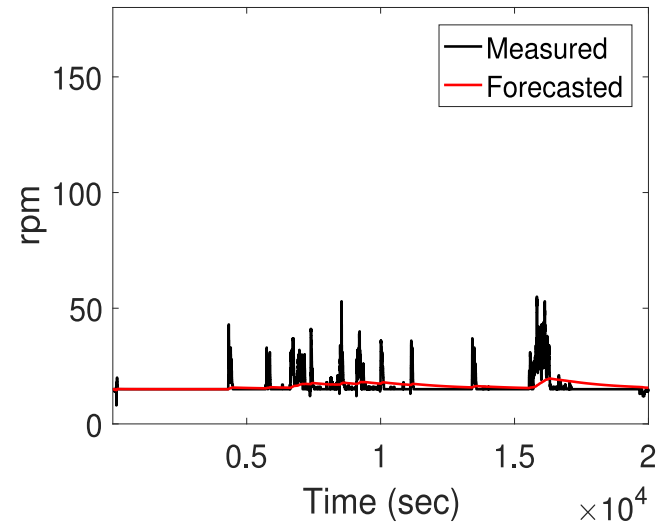


Fig. 21. Respiration Rate.

presence of other outliers and are not detected, and swamping occurs when normal observations are detected as abnormal (inversion).

The raised correlated alarms for this subject are presented in Figure 30, with the variations of whole physiological attributes to show the location of alarms with respect to changes in data. 5 alarms located exactly in the 5 zones of change are generated. The spikes with values outside the normal range in HR and the spikes with zero value in SpO2 are identified as faulty measurements, and do not trigger medical alarm as they are not correlated with other attributes.

Afterward, we conduct experiments to analyze the impact of forecasting on the detection accuracy, where we replace KF with several other forecasting procedures, namely: AutoRegressive Integrated Moving Average (ARIMA), Least Mean Square (LMS), Implicit Dynamic Feedback (IDF [53]) and Exponentially Weighted Moving Average (EWMA [54]). We tune the parameters of these algorithms in order to achieve

the nearest results. In fact, EWMA, IDF and KF are able to achieve the same forecasting performance after changing the configuration of their parameters. The forecasting procedure of EWMA is given in equation (23), in which we set $\alpha = 0.095$. We set the parameters $\beta = 0.095 \times 10^{-6}$ and $\delta = 10^{-10}$ in IDF forecasting procedure presented in equation (24) to provide the same result as KF and EWMA.

The used recursive equation for EWMA is:

$$Z_t = \alpha X_t + (1 - \alpha) Z_{t-1} \quad (23)$$

In the same manner, the recursive equation for IDF is:

$$\begin{aligned} \xi_t &= X_t - Z_t \\ I_t &= I_t + \xi_t \\ Z_{t+1} &= Z_0 + \beta \xi_t + \frac{\beta}{\delta} I_t \end{aligned} \quad (24)$$

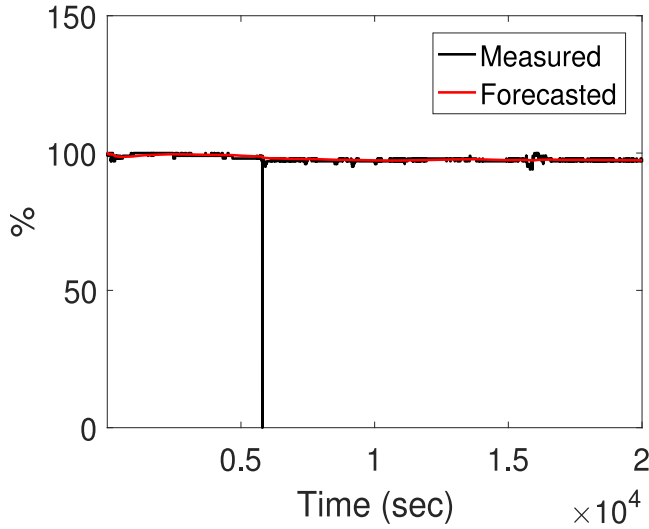


Fig. 22. SpO2.

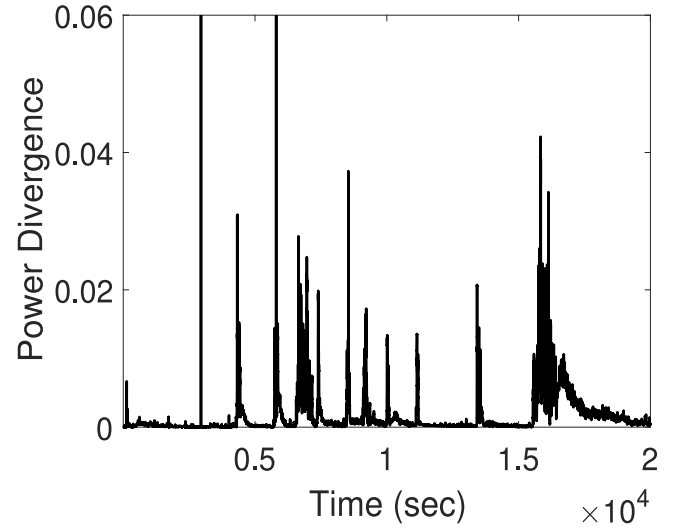


Fig. 24. PD.

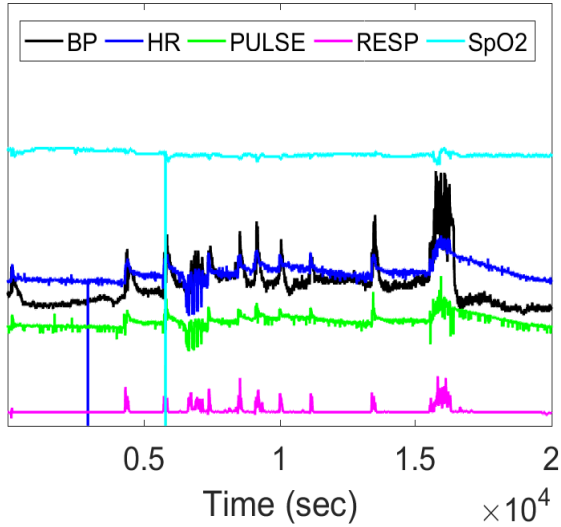


Fig. 23. Variations of 5 attributes.

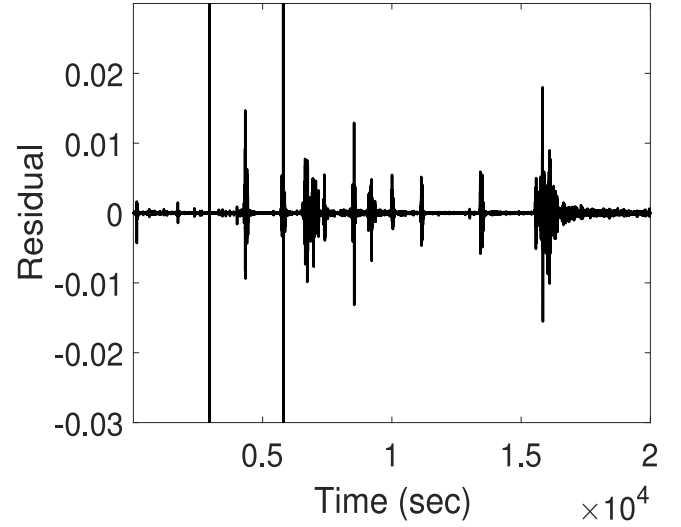


Fig. 25. Residual of PD.

The used ARIMA(p,d,q) model with minimal forecasting errors is:

$$Z_t = \mu + \varphi_1 X_{t-1} + \dots + \varphi_p X_{t-p} - \theta_1 \xi_{t-1} - \dots - \theta_q \xi_{t-q} \quad (25)$$

The LMS [55] uses a window containing N previous values $X_N = \{x_{1k}, x_{2k}, \dots, x_{Nk}\}$ to forecast the current value using randomly initiated weight vector W .

$$Z_t = W_{t-1}^T \cdot X_N \quad (26)$$

LMS uses an iterative algorithm for the correction of the weight vector W , as given in equation (27):

$$W_{t+1} = W_t + \mu \cdot (X_t - Z_t) \cdot X_N \quad (27)$$

where μ is a step size parameter that controls the convergence characteristics, and must be chosen with respect to the

condition in equation (28) for a fast convergence.

$$0 < \mu < \frac{2}{\lambda_{\max}} \quad (28)$$

where λ_{\max} is the largest eigenvalue of the product matrix $P_N = X_N \cdot X_N^T$ and updated online as given in equation (29):

$$\mu = \frac{1}{2 \times \text{trace}(P_N)} \quad (29)$$

To compare these forecasting procedures, we calculate the average of the mean-squared errors between forecasted and measured values:

$$MSE_j = \frac{1}{n} \sum_{i=1}^n (x_{ij} - z_{ij}) \quad (30)$$

In fact, ARIMA and LMS achieve good prediction and quickly react to changes in each attribute, in contrast to KF, EWMA and IDF, which have been tuned to derive a baseline of the attribute and remain relatively insensitive to deviations.

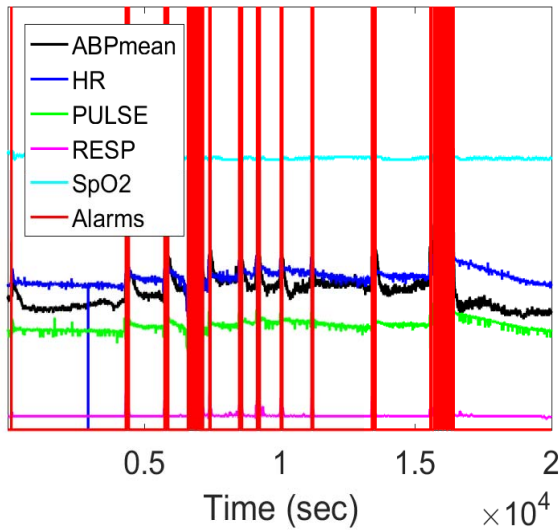


Fig. 26. Raised alarms.

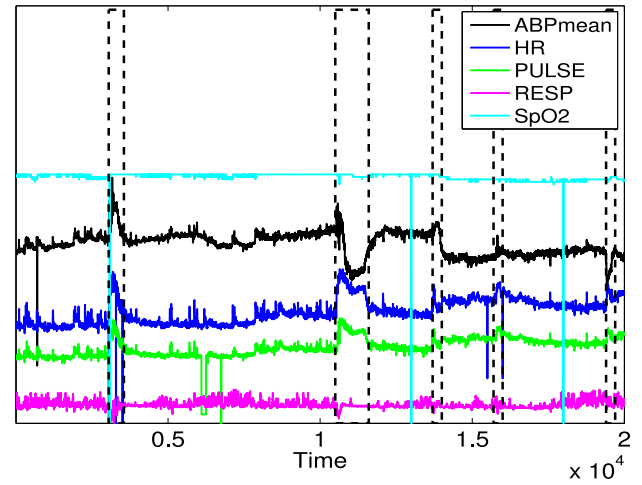


Fig. 28. Zone of changes.

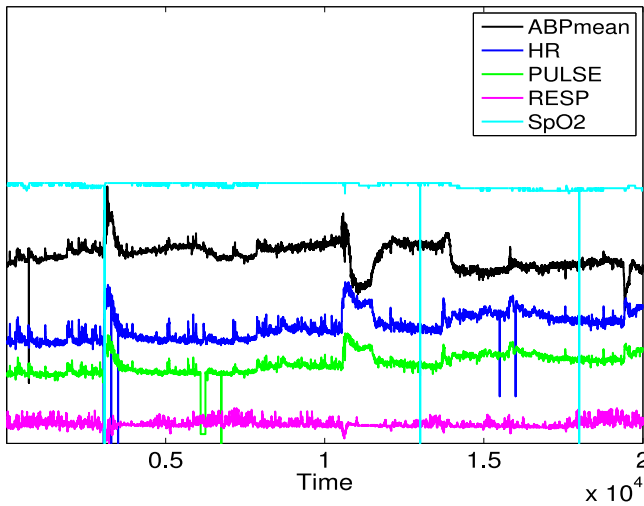


Fig. 27. Variations of 5 attributes.

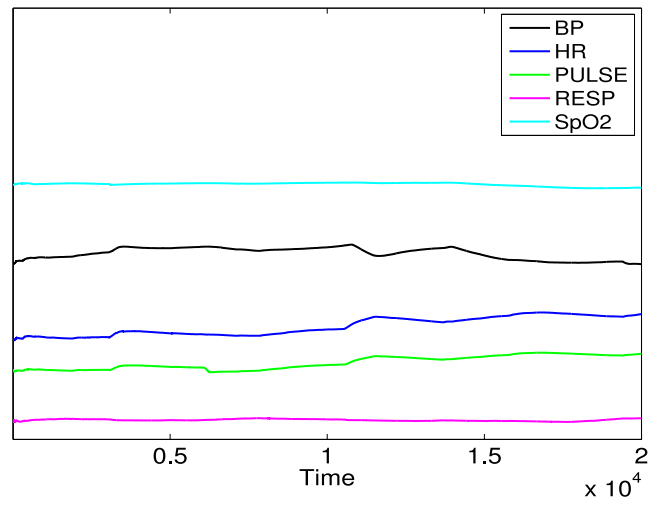


Fig. 29. Forecasted values.

Therefore, the rate of prediction error in Figure 31 is lower for ARIMA and LMS than KF, EWMA and IDF.

A. Performance Analysis

To analyze the performance of our proposed approach, we use the Receiver Operating Characteristic (ROC) to study the impact of the threshold on the Detection Rate and False Alarm Rate. The robust zscore is replaced by a threshold used to separate normal from abnormal measurements. The DR and FAR are given by the following equations:

$$DR = \frac{TP}{TP + FN} \quad (31)$$

$$FAR = \frac{FP}{FP + TN} \quad (32)$$

where TP, FP, FN and TN are the number of True Positives, False Positives, False Negatives and True Negatives respectively.

The ROC curve presented in Figure 32 shows the relationship between DR and the FAR for our proposed approach, which can achieve a DR of 100% with 6% of FAR. However, to demonstrate the effectiveness of our approach, we conduct comparisons with supervised classifications techniques, such as SVM and the decision tree (J48), as well as with Mahalanobis Distance (MD). We refer the reader to [56] for further details about the SVM classifier, [22] for the J48, [57] for the MD, and [58] for the robust estimation of the mean and the correlation matrix used to calculate MD.

1) *Comparison Result:* To prove the effectiveness of our proposed approach for WBANs, we compare our approach with several existing algorithms, such as SVM and J48 from ML based approaches, and MD from statistical based approaches. We tried to avoid developing them from scratch and used the WEKA toolkit to perform the analysis on SVM and J48, and MATLAB for MD. Figure 32 contains the obtained ROC for these 3 techniques, as well as for our proposed approach. We found that the performance of SVM

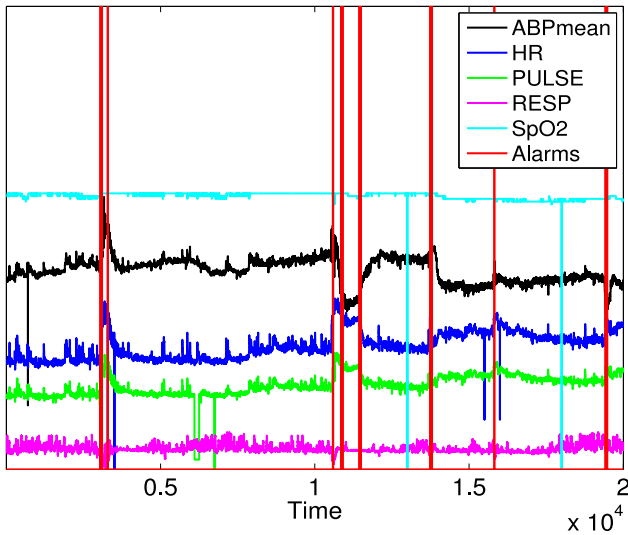


Fig. 30. Raised alarms.

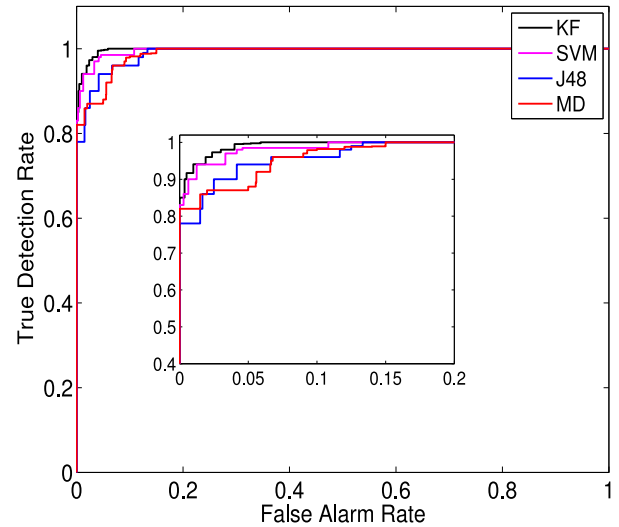


Fig. 32. ROC.

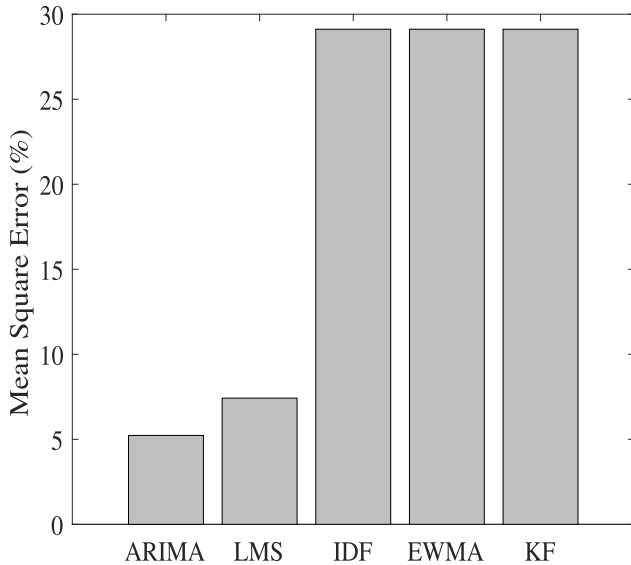


Fig. 31. Error rate with # forecasting.

is very close to our proposed approach achieving a detection rate of DR=100% with 8% of FAR for SVM (compared to 6% with our approach). The performance of SVM was followed by J48 (DR=100% with FAR = 13%) and finally MD (DR = 100% and FAR = 15%).

It is important to note that classification algorithms used in data mining, such as SVM and J48, require labeled training data set to derive an accurate classification model (hyperplane or tree). The training data are assumed to be correctly labeled as either normal or abnormal. In the real world however, labeled training data are often skewed or even unavailable. Skewed (or unbalanced) labeled data occurs when one class is over-represented (e.g., 99% of data are normal) and anomalies are almost not available in the training data set. Constructing a labeled training dataset is often a laborious and expensive task. It requires extensive experiments to determine applicable pre-processing and balancing algorithms.

When applying SVM, the computational complexity is $O(1)$ for classification. It is just a comparison with the hyperplane. However, the physiological parameters are dynamic, and the classification model needs to be updated. The required computational complexity to derive (or update) the classification model in SVM is $O(n^3)$ where n is the number of records in training phase. Therefore, the required complexity to derive (or update) the classification model in SVM may quickly deplete the energy of battery powered devices.

On the other hand, the computational complexity for classification using Decision tree J48 is $O(\log(n))$ which is higher than SVM, but the complexity to derive (or update) the decision tree is $O(nm\log(n))$. The computational complexity to inverse the covariance matrix in Mahalanobis distance is $O(n^3)$, which is greater than SVM and J48 algorithms.

The computational complexity of our proposed approach, which takes into account the correlations between physiological parameters is $O(m)$ that is more adequate for updating the reference model when compared to SVM and J48. SVM takes 42 seconds to rebuild the model from scratch. J48 needs to rebuild the entire tree from scratch to update the classification model, where this operation took 30 seconds in our experiments. The computational complexity required by OGK to derive anomaly free correlation matrix took 36 seconds, and the inversion of correlation matrix quickly consumes available energy in the LPU. Our proposed approach was able to achieve one cycle (forecasting, divergence and decision) in 11 seconds. The fact that our approach does not require labeled training data and its low computational complexity compared to previously cited algorithms, justifies its effectiveness in the context of WBANs.

V. CONCLUSION

In this paper, we have proposed a lightweight system for anomaly detection in medical WBANs, where faulty measurements and injected malicious data could threaten the life of the

monitored patient. The proposed system uses the divergence between measured and forecasted records. The change point detection is achieved by analyzing the residual of PD by a robust version of zscore. When the residual value is an outlier, a correlation analysis technique is activated to accurately distinguish faulty measurements from medical emergency, and a medical alarm is raised only when at least r attributes deviate simultaneously. This allows achieving spatial and temporal analysis, without prior knowledge of fault signatures or labelled training data.

Our approach is suitable for online detection and isolation of faulty or maliciously injected measurements with low computational complexity and storage requirement. We have tested our proposed approach on real physiological dataset publicly available on the Physionet Web site. The conducted experimental results demonstrate the efficiency and the accuracy of our approach, showing its ability to identify faulty measurements and reduce the number of false alarms.

We compared three existing approaches for anomaly detection (SVM, J48 and MD) with our system in terms of true positives and false alarm rate. We found the performance of our system slightly outperforms the SVM, which in turn outperforms the accuracy of J48 and MD. However, the computational complexity for building a classification model using SVM is $O(n^3)$, where n is the number of measurements in the training phase. Such complexity adds significant load and consumes scarce resources particularly depleting the limited LPU energy quickly. J48 is sensitive to small perturbations and its decision tree cannot be updated online. MD requires the derivation and the inversion of the correlation matrix, which needs higher amounts of resources and processing power.

As a future work, we intend to implement distributed detection on sensors to reduce energy wastage due to the transmission of normal and faulty measurements to the LPU, since the local processing of data consumes less energy than data transmission.

REFERENCES

- [1] J. Ko *et al.*, "MEDiSN: Medical emergency detection in sensor networks," *ACM Trans. Embedded Comput. Syst.*, vol. 10, no. 1, pp. 1–29, 2010.
- [2] A. Burns *et al.*, "SHIMMERTM—A wireless sensor platform for noninvasive biomedical research," *IEEE Sensor J.*, vol. 10, no. 9, pp. 1527–1534, Sep. 2010.
- [3] T. Yilmaz, R. Foster, and Y. Hao, "Detecting vital signs with wearable wireless sensors," *Sensors*, vol. 10, no. 12, pp. 10837–10862, 2010.
- [4] P. Humi, M. Anwander, G. Wagenknecht, T. Staub, and T. Braun, "TARWIS—A testbed management architecture for wireless sensor network testbeds," in *Proc. IEEE Netw. Oper. Manag. Symp.*, 2012, pp. 611–614.
- [5] O. Chipara, C. Lu, T. C. Bailey, and G.-C. Roman, "Reliable clinical monitoring using wireless sensor networks: Experiences in a step-down hospital unit," in *Proc. 8th ACM Conf. Embedded Netw. Sensor Syst. (SenSys)*, Zürich, Switzerland, 2010, pp. 155–168.
- [6] P. Kumar and H.-J. Lee, "Security issues in healthcare applications using wireless medical sensor networks: A survey," *Sensors*, vol. 12, no. 1, pp. 55–91, 2012.
- [7] V. P. Illiano and E. C. Lupu, "Detecting malicious data injections in event detection wireless sensor networks," *IEEE Trans. Netw. Service Manag.*, vol. 12, no. 3, pp. 496–510, Sep. 2015.
- [8] M. Won, S. M. George, and R. Stoleru, "Towards robustness and energy efficiency of cut detection in wireless sensor networks," *Ad Hoc Netw.*, vol. 9, no. 3, pp. 249–264, 2011.
- [9] H. Wang, H. Fang, L. Xing, and M. Chen, "An integrated biometric-based security framework using wavelet-domain HMM in wireless body area networks (WBAN)," in *Proc. IEEE Int. Conf. Commun. (ICC)*, Kyoto, Japan, 2011, pp. 1–5.
- [10] J. Ko *et al.*, "Wireless sensor networks for healthcare," *Proc. IEEE*, vol. 98, no. 11, pp. 1947–1960, Nov. 2010.
- [11] Q. Duan, S. Al-Haj, and E. Al-Shaer, "Provable configuration planning for wireless sensor networks," in *Proc. 8th Int. Conf. Netw. Service Manag. (CNSM)*, Las Vegas, NV, USA, 2012, pp. 316–321.
- [12] P. Kar and S. Misra, "Reliable and efficient data acquisition in wireless sensor networks in the presence of transfaulty nodes," *IEEE Trans. Netw. Service Manag.*, vol. 13, no. 1, pp. 99–112, Mar. 2016.
- [13] P. K. Sahoo, "Efficient security mechanisms for mHealth applications using wireless body sensor networks," *Sensors*, vol. 12, no. 9, pp. 12606–12633, 2012.
- [14] N. Shamaan, M. Shukor, N. Masdor, M. Sabullah, and M. Shukor, "Testing the normality of residuals on regression model for the growth of *Moraxella sp. B* on monobromoacetic acid," *Bull. Environ. Sci. Manag.*, vol. 3, no. 1, pp. 16–18, 2015.
- [15] D. Malan, T. Fulford-jones, M. Welsh, and S. Moulton, "CodeBlue: An ad hoc sensor network infrastructure for emergency medical care," in *Proc. Workshop Appl. Mobile Embedded Syst. (MobiSys)*, 2004, pp. 12–14.
- [16] K. F. Navarro, E. Lawrence, and B. Lim, "Medical MoteCare: A distributed personal healthcare monitoring system," in *Proc. Int. Conf. eHealth Telemed. Soc. Med. (eTELEMED)*, 2009, pp. 25–30.
- [17] J. P. S. Cunha *et al.*, "Vital-jacket[®]: A wearable wireless vital signs monitor for patients' mobility in cardiology and sports," in *Proc. Int. Conf. Pervasive Comput. Technol. Healthcare (PervasiveHealth)*, Munich, Germany, 2010, pp. 1–2.
- [18] H. Alemdar and C. Ersoy, "Wireless sensor networks for healthcare: A survey," *Comput. Netw.*, vol. 54, no. 15, pp. 2688–2710, 2010.
- [19] K. Grgić, D. Žagar, and V. Križanović, "Medical applications of wireless sensor networks—Current status and future directions," *Medicinski Glasnik*, vol. 9, no. 1, pp. 23–31, 2012.
- [20] G. Nychis, V. Sekar, D. G. Andersen, H. Kim, and H. Zhang, "An empirical evaluation of entropy-based traffic anomaly detection," in *Proc. 8th ACM SIGCOMM Conf. Internet Meas. (IMC)*, 2008, pp. 151–156.
- [21] A. Farrugia, G. L. Re, and M. Ortolani, "Probabilistic anomaly detection for wireless sensor networks," in *Proc. 12th Int. Conf. Artif. Intell. Around Man Beyond*, 2011, pp. 438–444.
- [22] X. Cheng, J. Xu, J. Pei, and J. Liu, "Hierarchical distributed data classification in wireless sensor networks," *Comput. Commun.*, vol. 33, no. 12, pp. 1404–1413, 2010.
- [23] K. Vu and R. Zheng, "Geometric algorithms for target localization and tracking under location uncertainties in wireless sensor networks," in *Proc. IEEE INFOCOM*, Orlando, FL, USA, 2012, pp. 1835–1843.
- [24] A. S. Raghuvanshi, R. Tripathi, and S. Tiwari, "Machine learning approach for anomaly detection in wireless sensor data," *Int. J. Adv. Eng. Technol.*, vol. 1, no. 4, pp. 47–61, 2011.
- [25] M. Xie, S. Han, B. Tian, and S. Parvin, "Anomaly detection in wireless sensor networks: A survey," *J. Netw. Comput. Appl.*, vol. 34, no. 4, pp. 1302–1325, 2011.
- [26] A. B. Sharma, L. Golubchik, and R. Govindan, "Sensor faults: Detection methods and prevalence in real-world datasets," *ACM Trans. Sen. Netw.*, vol. 6, no. 3, pp. 1–39, 2010.
- [27] R. Jurdak, X. R. Wang, O. Obst, and P. Valencia, "Wireless sensor network anomalies: Diagnosis and detection strategies," in *Intelligence-Based Systems Engineering*, A. Tolk and L. C. Jain, Eds. Heidelberg, Germany: Springer, 2011, ch. 12, pp. 309–325.
- [28] Y.-C. Chen and J.-C. Juang, "Outlier-detection-based indoor localization system for wireless sensor networks," *Int. J. Navig. Observation*, vol. 2012, pp. 1–11, Feb. 2012.
- [29] Y. Zhang, N. Meratnia, and P. J. M. Havinga, "Outlier detection techniques for wireless sensor networks: A survey," *IEEE Commun. Surveys Tuts.*, vol. 12, no. 2, pp. 159–170, 2nd Quart., 2010.
- [30] X. Miao, K. Liu, Y. He, Y. Liu, and D. Papadias, "Agnostic diagnosis: Discovering silent failures in wireless sensor networks," in *Proc. INFOCOM*, 2011, pp. 1548–1556.
- [31] Y. Zhang *et al.*, "Statistics-based outlier detection for wireless sensor networks," *Int. J. Geograph. Inf. Sci.*, vol. 26, no. 8, pp. 1373–1392, 2012.
- [32] S. Subramaniam, T. Palpanas, D. Papadopoulos, V. Kalogeraki, and D. Gunopulos, "Online outlier detection in sensor data using non-parametric models," in *Proc. 32nd Int. Conf. Very Large Data Bases (VLDB)*, 2006, pp. 187–198.

- [33] W. Wu *et al.*, "Localized outlying and boundary data detection in sensor networks," *IEEE Trans. Knowl. Data Eng.*, vol. 19, no. 8, pp. 1145–1157, Aug. 2007.
- [34] K. Ni and G. Pottie, "Sensor network data fault detection with maximum a posteriori selection and Bayesian modeling," *ACM Trans. Sensor Netw.*, vol. 8, no. 3, pp. 1–21, 2012.
- [35] Q. Yu, L. Jibin, and L. Jiang, "An improved ARIMA-based traffic anomaly detection algorithm for wireless sensor networks," *Int. J. Distrib. Sensors Netw.*, vol. 2016, Jan. 2016, Art. no. 28.
- [36] R. Mojarad, H. Kordestani, and H. R. Zarandi, "A cluster-based method to detect and correct anomalies in sensor data of embedded systems," in *Proc. 24th Euromicro Int. Conf. Parallel Distrib. Netw. Based Process. (PDP)*, 2016, pp. 240–247.
- [37] C. O'Reilly, A. Gluhak, M. A. Imran, and S. Rajasegarar, "Anomaly detection in wireless sensor networks in a non-stationary environment," *IEEE Commun. Surveys Tuts.*, vol. 16, no. 3, pp. 1413–1432, 3rd Quart., 2014.
- [38] L. M. A. Bettencourt, A. A. Hagberg, and L. B. Larkey, "Separating the wheat from the chaff: Practical anomaly detection schemes in ecological applications of distributed sensor networks," in *Proc. 3rd IEEE Int. Conf. Distrib. Comput. Sensor Syst. (DCOSS)*, Santa Fe, NM, USA, 2007, pp. 223–239.
- [39] F. Bao, I.-R. Chen, M. Chang, and J.-H. Cho, "Hierarchical trust management for wireless sensor networks and its applications to trust-based routing and intrusion detection," *IEEE Trans. Netw. Service Manag.*, vol. 9, no. 2, pp. 169–183, Jun. 2012.
- [40] F. Liu, X. Cheng, and D. Chen, "Insider attacker detection in wireless sensor networks," in *Proc. INFOCOM*, Barcelona, Spain, 2007, pp. 1937–1945.
- [41] P.-Y. Chen, S. Yang, and J. A. McCann, "Distributed real-time anomaly detection in networked industrial sensing systems," *IEEE Trans. Ind. Electron.*, vol. 62, no. 6, pp. 3832–3842, Jun. 2015.
- [42] Y. Zhang, N. Meratnia, and P. Havinga, "Adaptive and online one-class support vector machine-based outlier detection techniques for wireless sensor networks," in *Proc. Conf. Adv. Inf. Netw. Appl. Workshops*, Bradford, U.K., 2009, pp. 990–995.
- [43] S. Kumar, T. W. S. Chow, and M. G. Pecht, "Approach to fault identification for electronic products using Mahalanobis distance," *IEEE Trans. Instrum. Meas.*, vol. 59, no. 8, pp. 2055–2064, Aug. 2010.
- [44] A. Zjajo, *Stochastic Process Variation in Deep-Submicron CMOS*. Dordrecht, The Netherlands: Springer, 2016.
- [45] J. Hedengren and D. Brower, "Advanced process monitoring," in *Optimization and Analytics in the Oil and Gas Industry* (International Series in Operations Research and Management Science), K. C. Furman, J.-H. Song, and A. El-Bakry, Eds. Berlin, Germany: Springer, 2014.
- [46] D. Haussler and M. Opper, "Mutual information, metric entropy, and cumulative relative entropy risk," *Ann. Stat.*, vol. 25, no. 6, pp. 2451–2492, 1997.
- [47] T. M. Cover and J. A. Thomas, *Elements of Information Theory*. New York, NY, USA: Wiley, 1991.
- [48] J. Tang and Y. Cheng, "Quick detection of stealthy SIP flooding attacks in VoIP networks," in *Proc. IEEE Int. Conf. Commun. (ICC)*, Kyoto, Japan, 2011, pp. 1–5.
- [49] I. J. Taneja, "Bounds on triangular discrimination, harmonic mean and symmetric chi-square divergences," *J. Concrete Applicable Math.*, vol. 4, no. 1, pp. 91–111, 2006.
- [50] (Oct. 2017). *Engineering Statistics Handbook, Detection of Outliers*. [Online]. Available: <http://www.itl.nist.gov/div898/handbook/eda/section3/eda35h.htm>
- [51] (Oct. 2017). *Physionet*. [Online]. Available: <http://www.physionet.org/physiobank/database/mimicdb>
- [52] M. Saeed *et al.*, "Multiparameter intelligent monitoring in intensive care II (MIMIC-II): A public-access intensive care unit database," *Critical Care Med.*, vol. 39, no. 5, pp. 952–960, 2011.
- [53] J. D. Hedengren and A. N. Eaton, "Overview of estimation methods for industrial dynamic systems," *Optim. Eng.*, vol. 18, no. 1, pp. 155–178, 2017.
- [54] J. M. Lucas and M. S. Saccucci, "Exponentially weighted moving average control schemes: Properties and enhancements," *Technometrics*, vol. 32, no. 1, pp. 1–12, 1990.
- [55] S. Haykin, *Adaptive Filter Theory*, 4th ed. Upper Saddle River, NJ, USA: Prentice-Hall, 2001.
- [56] M. A. Hearst, S. T. Dumais, E. Osuna, J. Platt, and B. Scholkopf, "Support vector machines," *IEEE Intell. Syst. Appl.*, vol. 13, no. 4, pp. 18–28, Jul./Aug. 1998.

- [57] R. D. Maesschalck, D. Jouan-Rimbaud, and D. L. Massart, "The Mahalanobis distance," *Chemometrics Intell. Lab. Syst.*, vol. 50, no. 1, pp. 1–18, 2000.
- [58] P. J. Rousseeuw and K. van Driessen, "A fast algorithm for the minimum covariance determinant estimator," *Technometrics*, vol. 41, no. 3, pp. 212–223, 1999.



Osman Salem received the M.Sc. and Ph.D. degrees in computer science from Paul Sabatier University, Toulouse, France, in 2002 and 2006, respectively, and the Habilitation À Diriger des Recherches degree from the University of Paris Descartes, Paris, France, in 2016.

From 2006 to 2008, he was with the Department of Computer Science, Telecom Bretagne, Brest, France, as a Post-Doctoral Research Fellow. Since 2008, he has been an Associate Professor with the University of Paris Descartes. His research interests include security and anomaly detection in medical wireless sensor networks.



Ahmed Serhrouchni received the Ph.D. degree in computer science and the Habilitation À Diriger des Recherches degree from University Pierre and Marie Curie in 1989 and 2010, respectively. He is currently a Full Professor with Telecom ParisTech, CNRS-UMR 5141.

He is leading and involved in many research projects in network security in France and Europe. His research focuses on computer network security, security for vehicular networks, and security for industrial control system.



Ahmed Mehaoua received the M.Sc. and Ph.D. degrees in computer science from the University of Paris, France, in 1993 and 1997, respectively.

He is currently a Full Professor of computer communication with the Faculty of Mathematics and Computer Science, University of Paris Descartes, Paris, France. He is also the Head of the Department of Multimedia Networking and Security, LIPADE, a governmental computer science research center in Paris. His research interests include wireless healthcare systems and networks and applications.



Raouf Boutaba (F'12) received the M.Sc. and Ph.D. degrees in computer science from University Pierre and Marie Curie, Paris, France, in 1990 and 1994, respectively.

He is currently a Professor of computer science with the University of Waterloo, Waterloo, ON, Canada. His research interests include resource and service management in networks and distributed systems. He served as a Distinguished Speaker for the IEEE Computer and Communications Societies. He is the Founding Editor-in-Chief of the IEEE

TRANSACTIONS ON NETWORK AND SERVICE MANAGEMENT from 2007 to 2010, and is on the editorial boards of other journals. He is a fellow of the Engineering Institute of Canada and the Canadian Academy of Engineering.

Prof. Boutaba was a recipient of several best paper awards and other recognitions, such as the Premier's Research Excellence Award, the IEEE Hal Sobol Award in 2007, the Fred W. Ellersick Prize in 2008, the Joe LociCero and the Dan Stokesbury Awards in 2009, the Salah Aidarous Award in 2012, and the McNaughton Gold Medal in 2014.